Supplementary Information

Interlayer Proton Capture and Transport Mechanism in Oxygen Electrodes Boosts Proton Ceramic Electrolysis

Meijuan Fei[1,2], Zhaohui Cai[2], Peng Chen[1,2], Dongliang Liu[2], Cheng Huang[1,2], Jianqiu Zhu[3], Linjuan Zhang[3], Wei Wang[1,2], Chuan Zhou[1,2]*, Wei Zhou[1,2]*, Zongping Shao[4]*

[1]State Key Laboratory of Materials-Oriented Chemical Engineering, College of Chemical Engineering, Nanjing Tech University, Nanjing 211800, China.

[2]Suzhou Laboratory, Suzhou 215000, China.

[3]Key Laboratory of Interfacial Physics and Technology, Shanghai Institute of Applied Physics, Chinese Academy of Sciences, Shanghai 201800, China.

[4]Centre for Advanced Energy Material and Technologies, WA School of Mines, Curtin University, Perth, WA 6102, Australia.

*Corresponding author E-mail: zhouc@szlab.ac.cn (C. Zhou), zhouwei1982@njtech.edu.cn (W. Zhou), zongping.shao@curtin.edu.au.

Experimental section

Materials syntheses

The $Sr_3(Co_{0.8}Fe_{0.1}Nb_{0.1})_2O_{7-\delta}$ (SCFN-RP) and $SrCo_{0.8}Fe_{0.1}Nb_{0.1}O_{3-\delta}$ (SCFN-P) materials were synthesized via the sol–gel method. Niobium oxalate hydrate was initially dissolved by heating with deionized water and citric acid (CA), followed by the addition of other required metal nitrates until a clear solution was acquired. Among these, ethylenediaminetetraacetic acid (EDTA) and CA functioned as complexing agents, and an ammonia solution was used to adjust the pH to ~7. The precursor obtained from the dried gel was then subjected to calcination at 1000 °C for 10 h to obtain the desired powder. Simultaneously, the stoichiometric high-purity barium carbonate, zirconia, cerium oxide, yttrium oxide and ytterbium oxide were placed in the agate tank with ethanol, followed by ball milling (pulverisette 6, FRITSCH) at 400 rpm for 1 h. The $BaZr_{0.1}Ce_{0.7}Y_{0.1}Yb_{0.1}O_{3-\delta}$ (BZCYYb) electrolyte materials were then dried, crushed, and calcined at 1000 °C for 5 h.

Cell fabrication

The electrolyte powder was dry-pressed into a disc-shaped pellet and then sintered at 1475 °C for 10 h to obtain a dense electrolyte disc. The cathode powder was dispersed in a mixture of isopropyl alcohol, ethylene glycol and

glycerol at a ratio of 1 g:10 mL:2 mL:0.8 mL, followed by ball milling at a speed of 400 rpm for 30 min to prepare the cathode slurry, which was then sprayed onto the BZCYYb electrolyte disc and sintered at 1000 °C for 2 h to fabricate symmetric cells with the structure of the |BZCYYb|electrode electrode. The preparation of single cells with the Ni-BZCYYb |BZCYYb|electrode configuration is depicted below. First, the anode powder was prepared by mixing NiO, BZCYYb and soluble starch with a mass ratio of 6.5:3.5:1 via ball milling with ethanol at 400 rpm for 30 min. Second, 0.35 g of dried anode powder was pressed into the plate under a pressure of 1 MPa, and then 0.015 g of BZCYY electrolyte powder was evenly distributed on the anode surface and co-pressed at a pressure of 2 MPa, followed by calcination at 1475 °C for 10 h in air to obtain a Ni-BZCYYb anode-supported thin-film electrolyte single cell prepared by a dual dry-pressing and high-temperature sintering method. Finally, the cathode slurry was coated on the centre of the BZCYYb surface by the same method with an effective area of 0.25 cm^2 to obtain single cells.

Electrochemical measurements

A potentiostat (Solartron 1287) and a frequency response analyser (Solartron 1260) were used to perform EIS measurements to evaluate the electrochemical performance of the electrodes. The impedance values of the symmetrical cells were tested under dry air and various levels of steam. Different water pressures were controlled by adjusting the flow rate of the pump and the airflow. Among these, the stability and thermal cycling of the cell were tested under moist air provided by a gas wash bottle. The current–potential (I-V) polarization curve and the power density (I-P) curve of single cells were acquired using a Keithley 2420 based on a four-probe configuration. In the FC mode, the air electrode side was exposed to air at a flow rate of 100 mL $min^{-1,}$ and the anode side supplied dry hydrogen and was maintained at 80 mL min^{-1}. In the EC mode, steam at different flow rates was fed into the air electrode side, and the fuel electrode was also purged with hydrogen at a rate of 80 mL min^{-1}.

Characterizations

X-ray diffraction (XRD, D8 Advance Bruker) with Cu-Kα radiation was used to analyse the crystal structure of the powder. Thermogravimetric analysis (TGA, Netzsch, STA 449 F3) was carried out to detect the changes in weight loss under flowing air from room temperature to 1000 °C at a heating rate of 5 °C min^{-1}. The crystal structure of the SCFN-RP samples after steam treatment was determined via microcrystal electron diffraction (MicroED) following treatment with 20 vol.% H_2O–air at 600 °C. Data collection was performed using a JEM-2100 Plus transmission electron microscope (JEOL, Japan) with an acceleration voltage of 200 kV, a wavelength of 0.0025079 nm, and a MerelinEM high-speed direct electron camera. A QUANTIFOIL copper grid (R1.2/1.3), a Fischione 2550 cryo-transfer holder, and an ambient temperature of 77 K were used along with a PELCO easiGlow™ glow discharge system. In situ Fourier transform infrared spectroscopy (FTIR) measurements were conducted using a Spectrum 3 FTIR spectrometer (PerkinElmer) equipped with a Harrick Praying Mantis accessory, covering a frequency range of 2600–3000 cm^{-1} with a resolution of 2 cm^{-1}. The perovskite powder was mixed with KBr at a weight ratio of 1:100 to increase the intensity of the infrared signals. The sample was stabilized in dry air at 600 °C for 30 min, followed by the introduction of 20 vol.% H_2O–air to begin the FTIR measurements. High-temperature hard X-ray absorption spectroscopy (XAS) was performed at the BL14W beamline at the Shanghai Synchrotron Radiation Facility (SSRF). The samples were also treated at 600 °C for 2 h under both dry air and 20 vol.% H_2O–air, followed by quenching. The

concentrations of the protons and hydroxyl groups in the surface and bulk phases were analysed by time-of-flight secondary ion mass spectrometry (TOF-SIMS). The samples were also treated at 600 °C for 2 h under both dry air and 20 vol.% H_2O–air, followed by quenching. The surface and cross-sectional morphologies of the powders and cells were examined by scanning electron microscopy (SEM, JEOL-S4800). The chemical composition and surface elemental states of the samples were identified using X-ray photoelectron spectroscopy (XPS, MULT1LAB2000, VG). The H_2O desorption (H_2O-TPD) characteristics of the synthesized material were evaluated via mass spectrometry (Hiden Analytical HPR-20) from room temperature to 1000 °C. H_2O-TPD data were obtained after the powder was pretreated at 250 °C for 2 h under 10 vol.% H_2O–air.

DFT calculation method

Density functional theory (DFT) calculations were conducted using the Vienna Ab initio Simulation Package (VASP 5.4.4) in the Hygon platform with two AMD 7742 64-core processors, employing the Perdew–Burke–Ernzerhof (PBE) functional within the generalized gradient approximation (GGA) for electron exchange and correlation. The core-valence electron interactions were represented with projector-augmented wave (PAW) potentials, utilizing a plane wave basis set with a kinetic energy cut-off of 500 eV. van der Waals interactions were incorporated using the DFT-D3 method of Grimme to accurately describe the hydrogen bonding and water adsorption effects. Electronic energy convergence was achieved when the energy change between successive iterations was less than 10–5 eV, whereas geometry optimization was deemed convergent when forces on each atom were less than 0.03 eV/Å. Brillouin zone sampling was performed using the Monkhorst–Pack scheme with a k-point mesh of size 8 × 8 × 1 for the $Sr_3Co_3O_{17-x}(OH)_x \cdot \alpha H_2O$ system. Spin polarization effects were included in all calculations to account for the magnetic properties of the cobalt-containing framework properly.

The proton migration pathways were investigated using the nudged elastic band (NEB) method with three intermediate images between the initial and final states. The climbing image nudged elastic band (CI-NEB) approach was employed to locate transition states accurately along the migration pathways. Structural relaxations were performed using the direct inversion of the iterative subspace (DIIS) algorithm, with a maximum of 100 ionic steps allowed for convergence. The migration energy barriers were calculated as the energy difference between the transition state and the initial configuration, providing insights into the kinetic feasibility of proton diffusion processes in the layered cobaltate structure.

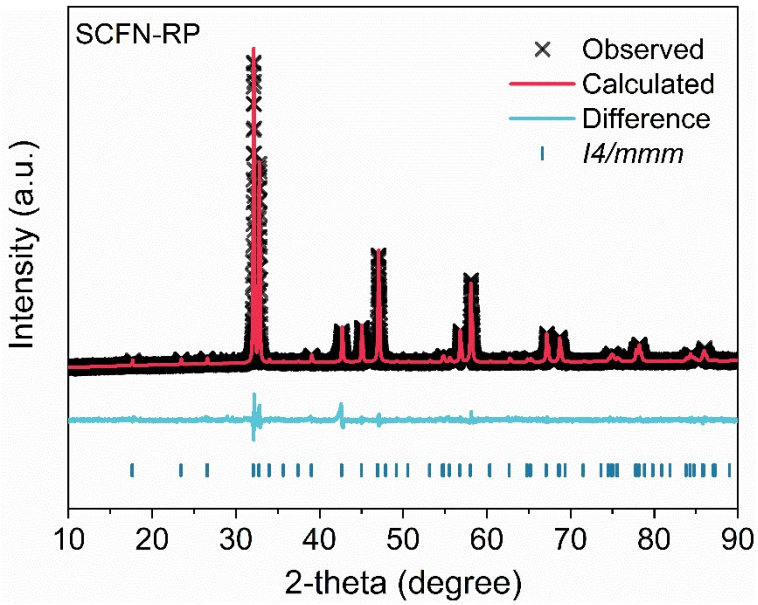

Fig. S1 XRD patterns with refinement plots of SCFN-RP.

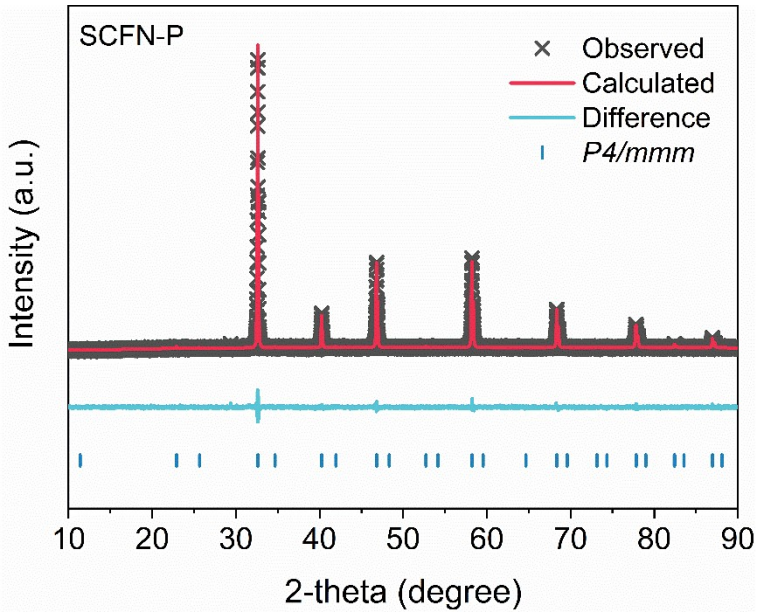

Fig. S2 XRD patterns with refinement plots of SCFN-P.

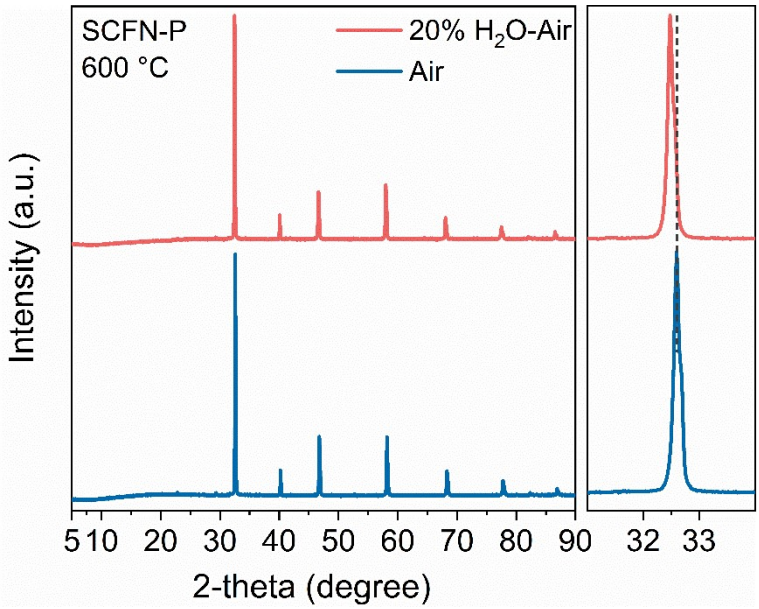

Fig. S3 XRD profiles for SCFN-P after treatment at 600 °C for 2 h under dry air and 20 vol.% H_2O–air.

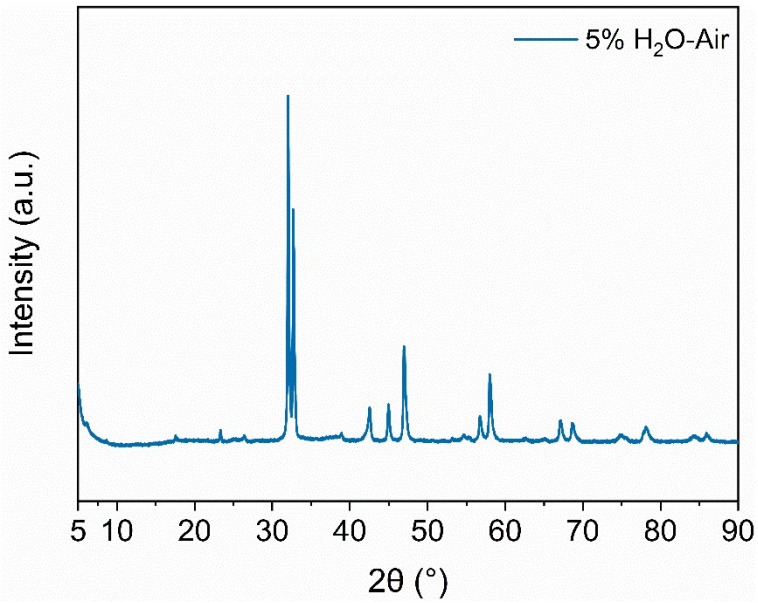

Fig. S4 XRD profiles for SCFN-RP sample after treatment at 600 °C for 1 h under 5 vol.% H_2O–air.

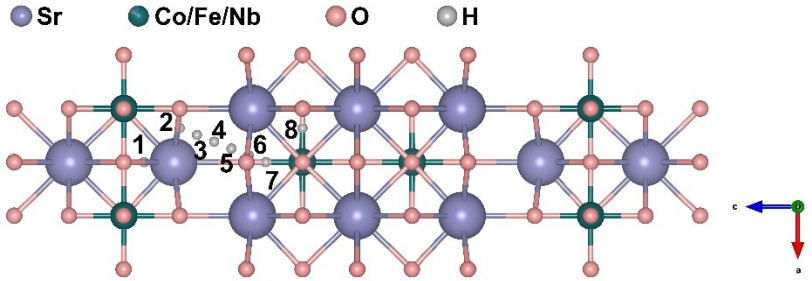

Fig. S5 The structural diagram and proton transport pathway for the fresh SCFN-RP sample.

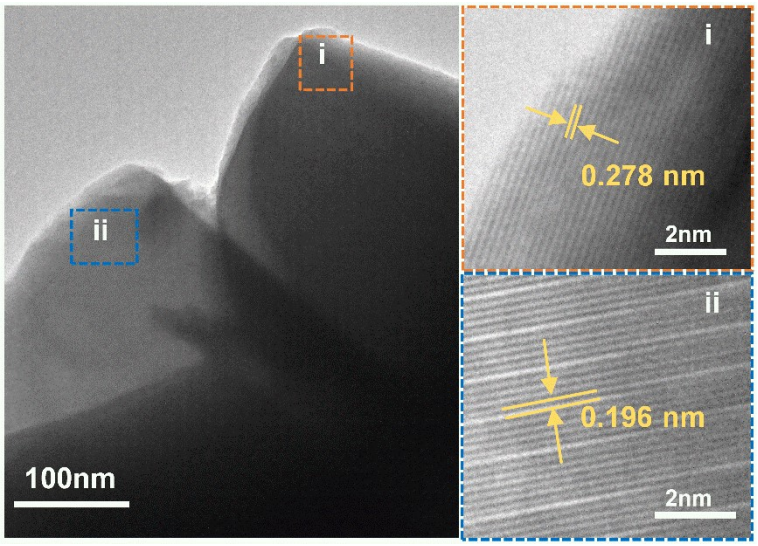

Fig. S6 HR-TEM image for the SCFN-RP sample, (i) and (ii), show the zoomed-in view of the corresponding positions respectively (scale bar is 2 nm).

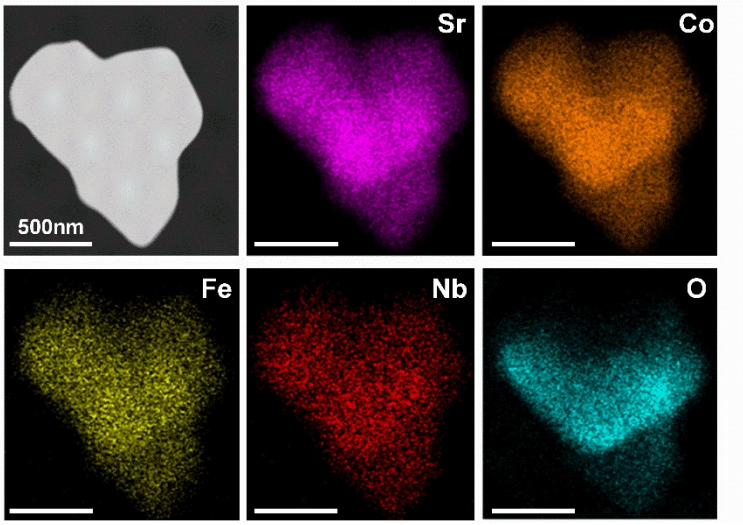

Fig. S7 TEM-EDX element mapping for the SCFN-RP sample.

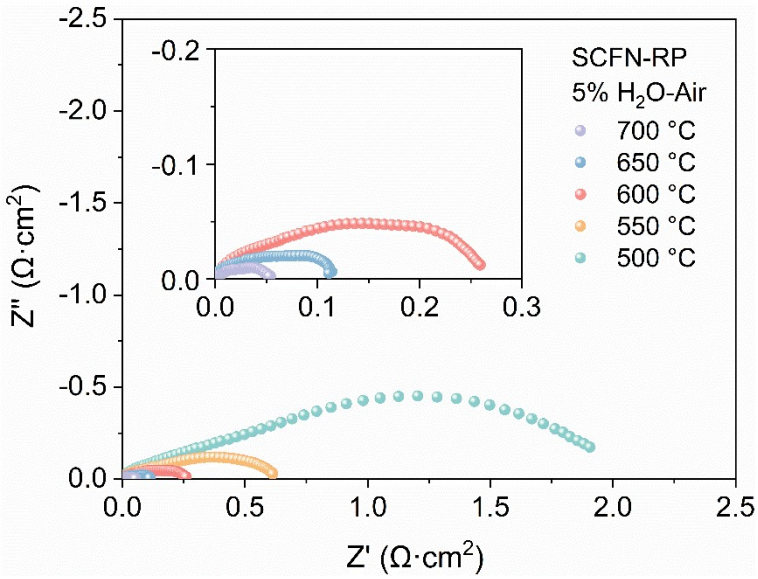

Fig. S8 EIS plots of BZCYYb supported symmetric cell with SCFN-RP electrode at 500-700 °C under 5 vol.% H_2O–air.

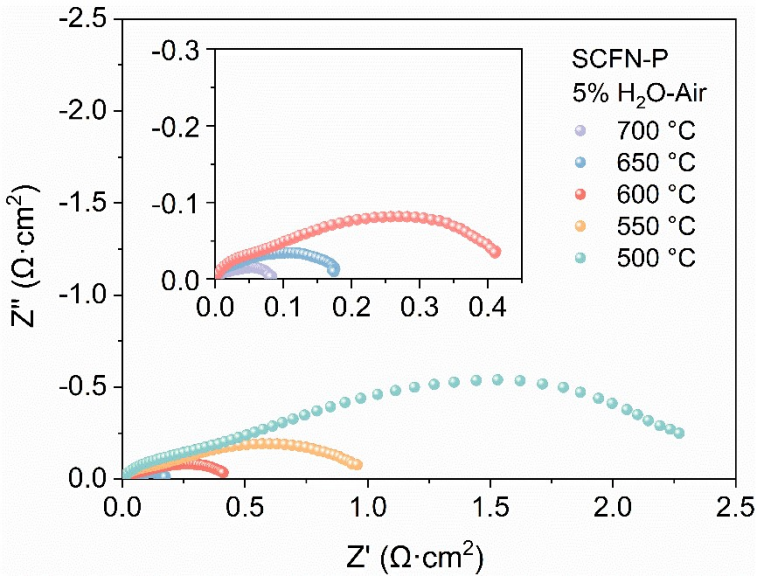

Fig. S9 EIS plots of BZCYYb supported symmetric cell with SCFN-P electrode at 500-700 °C under 5 vol.% H_2O–air.

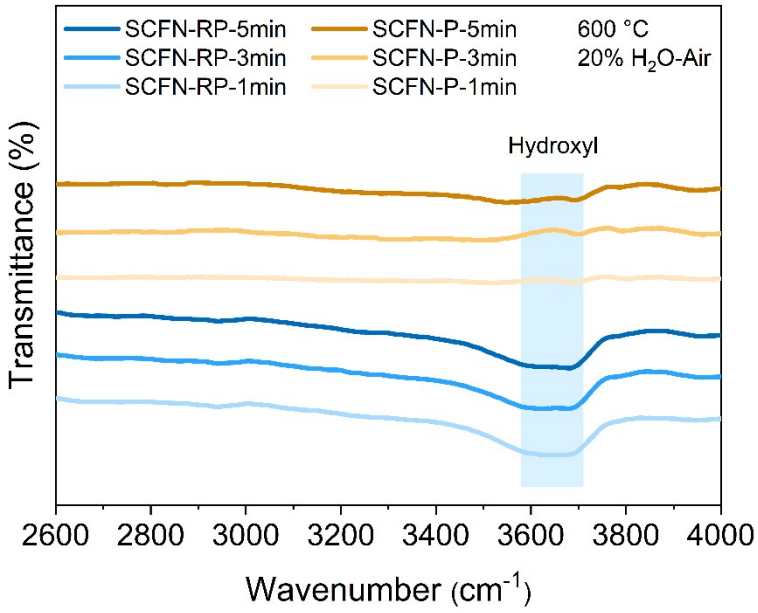

Fig. S10 In situ FTIR spectra for the SCFN-RP and SCFN-P samples tested at 600 °C at different times under 20 vol.% H_2O–air.

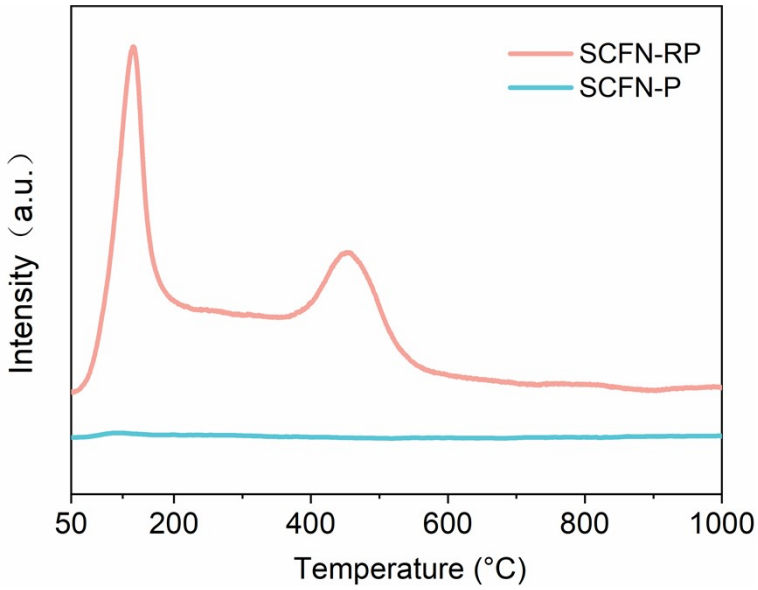

Fig. S11 The H_2O-TPD of SCFN-RP and SCFN-P samples after treatment at 250 °C for 2 h under 10 vol.% H_2O–air.

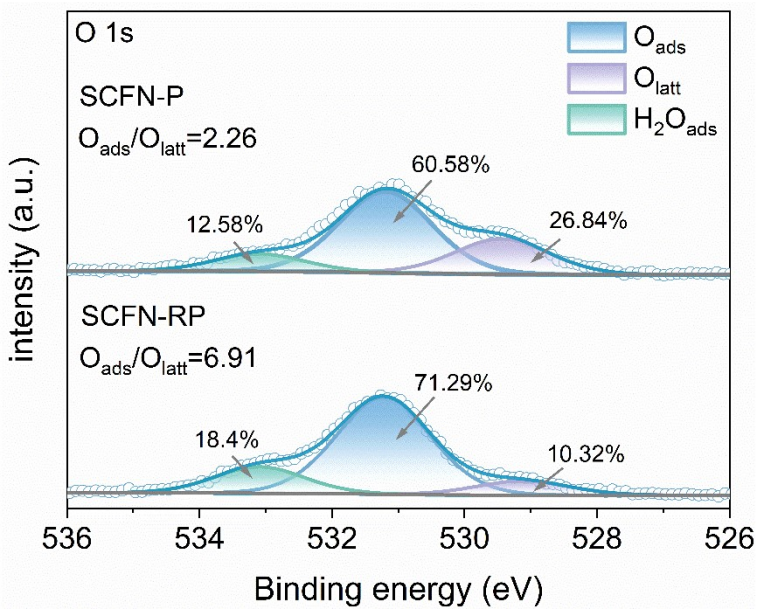

Fig. S12 XPS spectra of the SCFN-RP and SCFN-P samples showing the O 1s structures.

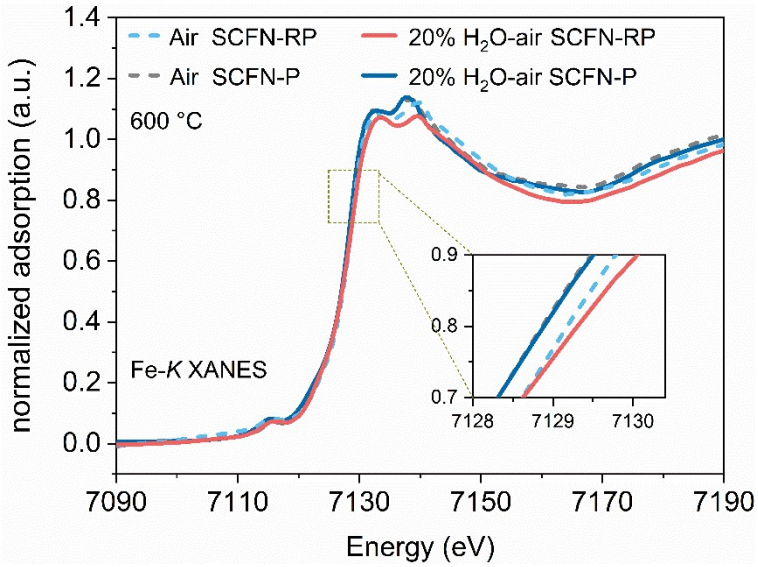

Fig. S13 Fe K-edge XANES spectra for the SCFN-RP and SCFN-P samples under different operating conditions.

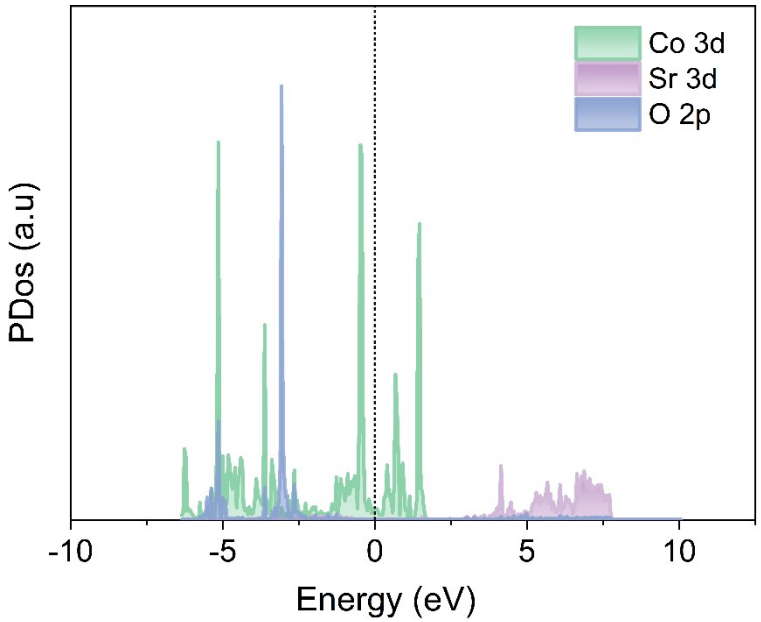

Fig. S14 Projected Density of States (PDOS) of Co 3d, Sr 3d, and O 2p Orbitals in SCFN-RP.

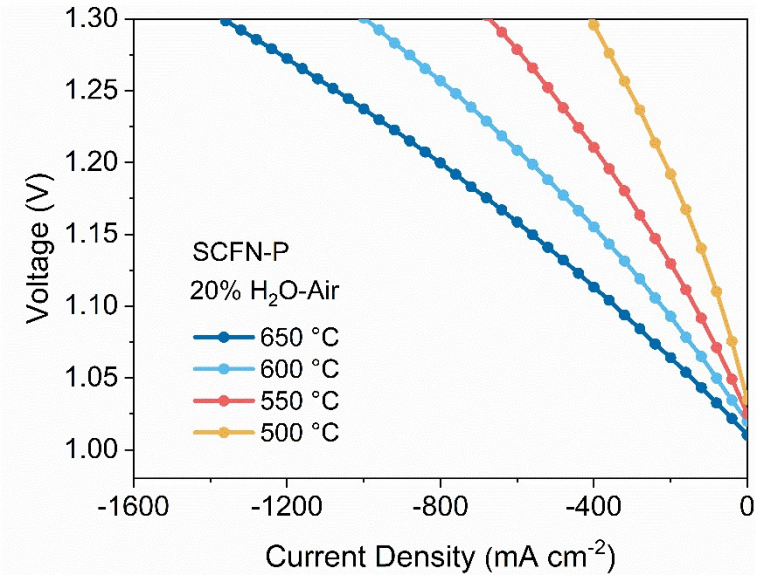

Fig. S15 I–V curves of a single cell with the SCFN-P oxygen electrode in the PCEC mode at 500-650 °C.

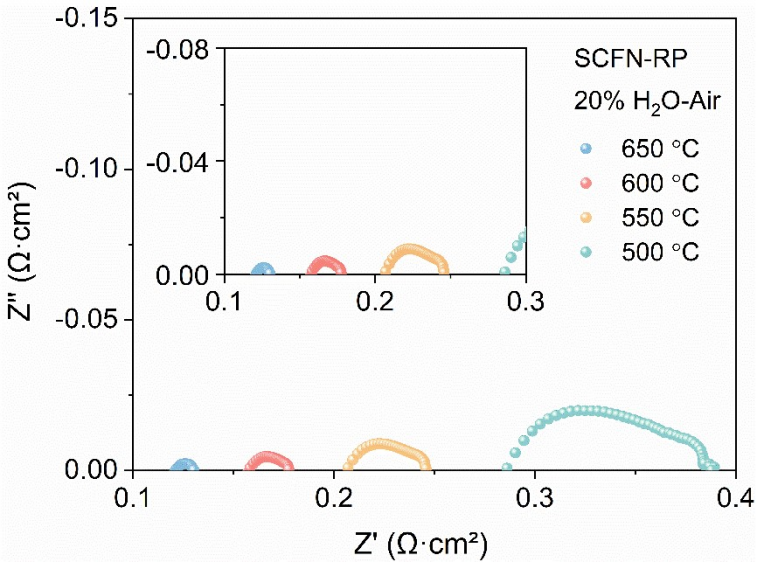

Fig. S16 EIS curves of a single cell in the PCEC mode (at 1.3V) at 500-650 °C for the SCFN-RP electrode.

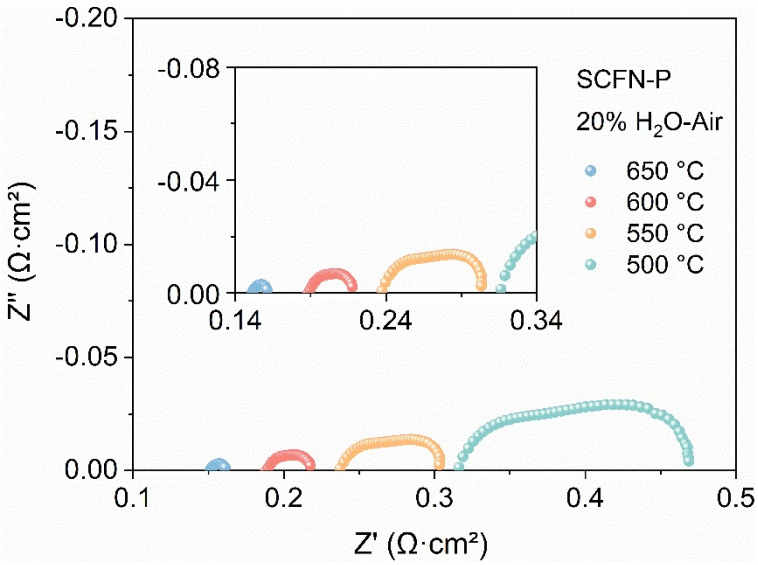

Fig. S17 EIS curves of a single cell in the PCEC mode (at 1.3V) at 500-650 °C for the SCFN-P electrode.

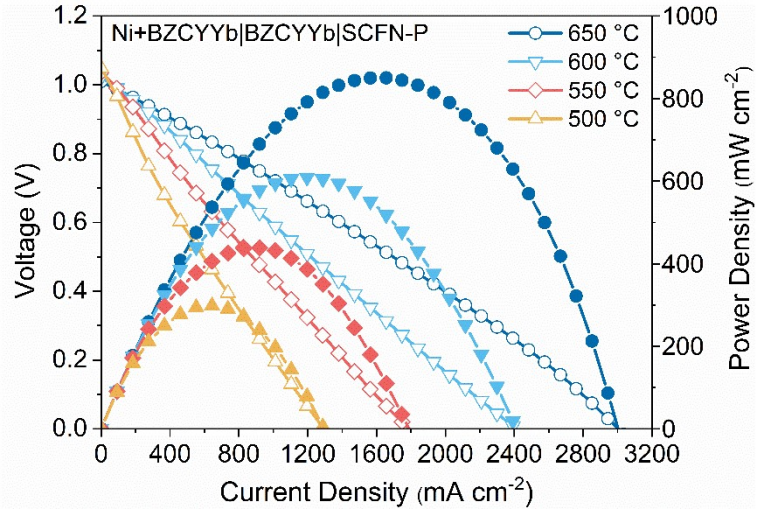

Fig. S18 I-V and I-P curves of a single cell with the SCFN-P electrode in the PCFC mode.

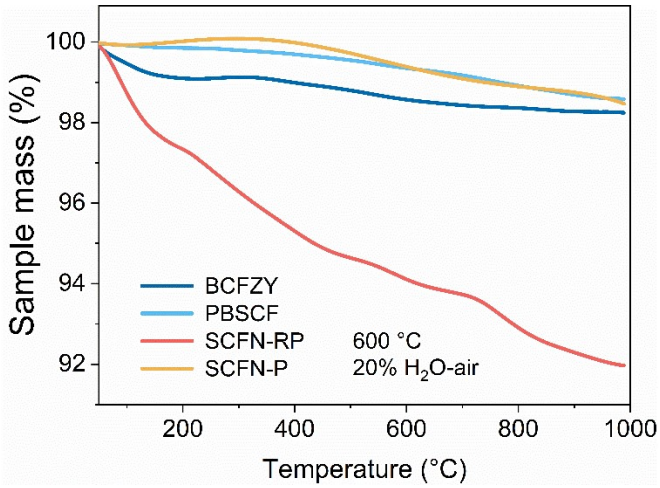

Fig. S19 TGA curves of different samples from room temperature to 1000 °C under 20 vol.% H_2O–air.

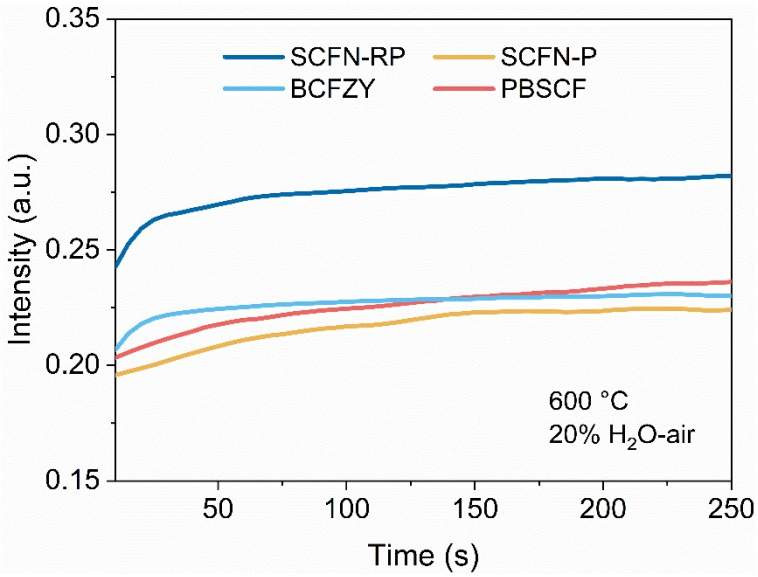

Fig. S20 TOF-SIMS depth profiles of –OH under negative ion mode for different samples.

Table S1 The full width at half maximum (FWHM) of the main XRD peak of the SCFN-RP sample under different atmospheres.

Temperature (°C)	Atmosphere	Time (min)	FWHM (° 2Theta)
600	Dry air	30	0.24557
600	Dry air	50	0.24592
600	20 vol.% H_2O–air	75	0.24293
600	20 vol.% H_2O–air	95	0.23085
600	20 vol.% H_2O–air	115	0.24767
600	Dry air	145	0.24287
600	Dry air	165	0.23403
600	Dry air	185	0.24014

Table S2. Three datasets individually collected by MicroED of the SCFN-RP sample treated by 20 vol.% H_2O–air at 600 °C for 2 h.

data	a/Å	b/Å	c/Å	α/°	β/°	γ/°	$CC_{1/2}$	Compl./%	I/σ	Ntotal	Nunique	Rmeas
1	3.84	3.84	42.9	90	90	90	95.0*	62.70%	3.96	606	163	27.50%
2	3.82	3.82	40.84	90	90	90	95.9*	93.50%	3.27	519	230	26.90%
3	3.86	3.86	41.77	90	90	90	97.0*	68.90%	4.16	697	173	24.50%

Table S3. Crystallographic and Refinement Information of SCFN-RP treated by 20 vol.% H_2O–air at 600 °C for 2 h.

Empirical formula	$Co_2O_{30}Sr_3$
Formula weight	978.56
Temperature/K	77
Crystal system	tetragonal
Space group	I4/mmm
a/Å	3.8400(5)
b/Å	3.8400(5)
c/Å	42.250(8)
α/°	90
β/°	90
γ/°	90
Volume/Å^3	623.0(2)
Z	1
ρ_{calc}g/cm^3	2.608
Radiation	Electron (λ = 0.02508)
2Θ range for data collection/°	0.136 to 1.796
Index ranges	$-4 \leq h \leq 4$, $-4 \leq k \leq 4$, $-46 \leq l \leq 49$
Reflections collected	2397
Independent reflections	247 [R_{int} = 0.3045, R_{sigma} = 0.2115]
Data/restraints/parameters	247/0/10
Goodness-of-fit on F^2	2.829
Final R indexes [I>=2σ (I)]	R_1 = 0.3863, wR_2 = 0.6783
Final R indexes [all data]	R_1 = 0.3905, wR_2 = 0.6881

Table S4. Fractional Atomic Coordinates ($\times 10^4$) and Equivalent Isotropic Displacement Parameters ($Å^2 \times 10^3$) for SCFN-RP treated by 20 vol.% H_2O–air at 600 °C for 2 h.

Atom	x	y	z	U(eq)
Sr01	10000	10000	5000	20
Co02	5000	5000	4558(5)	20
Sr03	0	10000	4162(10)	29
O1	0	0	2272(9)	10
O2	5000	5000	3372(11)	10
O006	5000	5000	5000	10
O4	0	0	2966(12)	10
O008	5000	5000	4037(10)	10
O00A	5000	10000	4566(7)	10
O3	5000	0	3746(14)	10

Table S5. Bond Lengths for SCFN-RP treated by 20 vol.% H_2O–air at 600 °C for 2 h.

Atom	Atom	Length/Å
Co02	O006	1.87(2)
Co02	O008	2.20(5)
Co02	O00A	1.9203(8)
Co02	O00A[1]	1.9203(7)
Co02	O00A[2]	1.9203(8)
Co02	O00A[3]	1.9203(7)

Table S6. Bond Angles for SCFN-RP treated by 20 vol.% H_2O–air at 600 °C for 2 h.

Atom	Atom	Atom	Angle/°
O006	Co02	O008	180
O006	Co02	O00A	89.0(11)
O006	Co02	O00A[1]	89.0(11)
O006	Co02	O00A[2]	89.0(11)
O006	Co02	O00A[3]	89.0(11)
O00A[1]	Co02	O008	91.0(11)
O00A	Co02	O008	91.0(11)
O00A[2]	Co02	O008	91.0(11)
O00A[3]	Co02	O008	91.0(11)
O00A	Co02	O00A[2]	89.98(4)
O00A[3]	Co02	O00A[1]	89.98(4)
O00A	Co02	O00A[3]	89.98(4)
O00A[3]	Co02	O00A[2]	178(2)
O00A	Co02	O00A[1]	178(2)
O00A[2]	Co02	O00A[1]	89.98(4)
Co02[4]	O006	Co02	180
Co02[5]	O00A	Co02	178(2)

Table S7. The ASR values of different oxygen electrodes in wet air at 550-650 °C.

Oxygen Electrodes	Electrolyte	Atmosphere	ASRs (Ω cm^2)			Refs.
			650 °C	600 °C	550 °C	
PBCC-BCO	BZCYYb1711	3%H_2O–air	0.05	0.24	0.51	[33]
PBCCHf0.1	BZCYYb1711	3%H_2O–air	0.11	0.27	0.55	[27]
BaGdPrCo	BZCYYb1711	3%H_2O–air	0.14	0.27	0.67	[34]
2W-PBSCF	BZCYYb1711	3%H_2O–air	0.24	0.36	0.8	[32]
BaGdCo0.1	BZCYYb3511	3%H_2O–air	0.23	0.43	1	[21]
SCFN-RP	BZCYYb1711	5%H_2O–air	0.12	0.26	0.63	This work
P2.7NCNO	BZCYYb1711	3%H_2O–air	0.1	0.25	0.67	[20]
PNCO-64	BZCYYb1711	3%H_2O–air	0.14	0.34	0.82	[8]
LSCF2.7	BZCY172	Wet	0.19	0.42	1.15	[25]
D-SFN	BZCYYb1711	3%H_2O–air	0.15	0.4	1.21	[28]
BCCY	BZCYYb1711	2.5%H_2O–air	0.08	0.25	0.49	[5]
D-BFZ	BZCYYb1711	3%H_2O–air	0.11	0.23	0.51	[26]
BSCFP0.05	BZCYYb1711	5%H_2O–air	0.24	0.38	0.66	[23]
C/H-BSCF	BZCYYb1711	3%H_2O–air	0.11	0.26	0.68	[6]
HE-PBSLCC	BZCYYb1711	3%H_2O–air	0.12	0.26	0.75	[3]
NSTF0.3	BZCYYb1711	5%H_2O–air	0.19	0.33	0.77	[7]
PLNBSCC	BZCYYb1711	5%H_2O–air	0.16	0.35	0.81	[23]
BLFZN0.1	BZCYYb1711	3%H_2O–air	0.05	0.21	0.921	[29]
BCFZY	BZCYYb1711	Wet	0.35	0.62	1.05	[19]
2Ru-BCF	BZCYYb1711	3%H_2O–air	0.17	0.48	1.19	[31]
BSSNC	BZCY172	3%H_2O–air	0.25	0.66	1.52	[30]
PBCFC	BZCYYb1711	Wet	0.5	1	2.15	[22]

Electrolytes: BZCYYb1711: $BaZr_{0.1}Ce_{0.7}Y_{0.1}Yb_{0.1}O_{3-\delta}$; BZCYYb3511: $BaZr_{0.3}Ce_{0.5}Y_{0.1}Yb_{0.1}O_{3-\delta}$; BZCY172: $BaZr_{0.1}Ce_{0.7}Y_{0.2}O_{3-\delta}$;
Oxygen electrode: PBCC-BCO: $PrBa_{0.8}Ca_{0.2}Co_2O_{5+\delta}$; PBCCHf0.1: $PrBa_{0.8}Ca_{0.2}Co_{1.9}Hf_{0.1}O_{5+\delta}$; BaGdPrCo: $Ba_{0.8}Gd_{0.8}Pr_{0.4}Co_2O_{5+\delta}$
2W-PBSCF: 2 wt% W-$PrBa_{0.5}Sr_{0.5}Co_{1.5}Fe_{0.5}O_{5+\delta}$; BaGdCo0.1: $Ba_{1.1}Gd_{0.9}Co_2O_{6-\delta}$; P2.7NCNO: $Pr_{2.7}Ni_{1.6}Cu_{0.3}Nb_{0.}1O_{7-\delta}$;
PNCO-64: $Pr_2Ni_{0.6}Co_{0.4}O_{4-\delta}$; LSCF2.7: $LaSr_{2.7}Co_{1.5}Fe_{1.5}O_{10-\delta}$; D-SFN: $Sr_{2.8}Fe_{1.8}Nb_{0.2}O_{7-\delta}$; BCCY: $BaCo_{0.7}(Ce_{0.8}Y_{0.2})_{0.3}O_{3-\delta}$
D-BFZ: $Ba_{0.875}Fe0._{875}Zr_{0.125}O_{3-\delta}$; BSCFP0.05: $Ba_{0.5}Sr_{0.5}(Co_{0.8}Fe_{0.2})_{0.95}P_{0.05}O_{3-\delta}$; C/H-BSCF: $Ba_{1.5}Sr_{1.5}Co_{1.6}Fe_{0.4}O_{7-\delta}$;
HE-PBSLCC: $Pr_{0.2}Ba_{0.2}Sr_{0.2}La_{0.2}Ca_{0.2}CoO_{3-\delta}$; NSTF0.3: $Na_{0.3}Sr_{0.7}Ti_{0.1}Fe_{0.9}O_{3-\delta}$; PLNBSCC: $Pr_{1/6}La_{1/6}Nd_{1/6}Ba_{1/6}Sr_{1/6}Ca_{1/6}CoO_{3-\delta}$
BLFZN0.1: $Ba_{0.95}La_{0.05}(Fe_{0.8}Zn_{0.2})_{0.}9Ni_{0.1}O_{3-\delta}$; BCFZY: $BaCo_{0.4}Fe_{0.4}Zr_{0.1}Y_{0.1}O_{3-\delta}$; 2Ru-BCF: 2 wt.% Ru-$BaCe_{0.125}Fe_{0.875}O_{3-\delta}$;
BSSNC: $Ba_{0.5}Sr_{0.5}Sc_{0.175}Nb_{0.025}Co_{0.8}O_{3-\delta}$; PBCFC: $Pr_{0.6}Ba_{0.2}Ca_{0.2}Fe_{0.8}Co_{0.2}O_{3-\delta}$

Table S8. PPD values of different oxygen electrodes operating in the PCFC mode at 500-600 °C.

Oxygen electrode	Electrolyte	thickness (μm)	Atmosphere	PPD (W cm^{-2})			Refs.
				600 °C	550 °C	500 °C	
PNCO-64	BZCYYb1711	10	3%H_2O–H_2/Air	0.86	0.58	/	[8]
PBCFS05	BZCYYb4411	6-7	3%H_2O–H_2	1.12	0.69	/	[49]
SCFN-RP	BZCYYb1711	10	H_2/Air	0.92	0.63	0.41	This work
PBCC-BCO	BZCYYb1711	10	3%H_2O–H_2/Air	1.06	0.66	/	[33]
PBCsC	BZCYYb1711	8	3%H_2O–H_2/Air	1.19	0.72	0.41	[48]
BCFZYMg	BZCYYb1711	16	H_2/Air	0.85	0.66	0.48	[43]
BB-OPS	BZCYYb1711	22	H_2/Air	0.88	0.63	0.43	[44]
N-BCFZYNF	BZCYYb1711	10.79	H_2/3%H_2O–air	0.78	0.55	0.37	[40]
BSCFP0.05	BZCYYb1711	16	H_2/Air	0.84	0.64	0.43	[23]
PSFN/Fe_2O_3	BZCYYb1711	10	3%H_2O–H_2/Air	0.52	0.33	/	[46]
D-SFN	BZCYYb1711	23	H_2/Air	0.48	0.36	0.24	[28]
PBSCF	BZCYYb4411	15	3%H_2O-H_2/3%H_2O–air	0.85	0.6	0.39	[41]
BSCFF	BZCYYb1711	16.6	H_2/Air	0.67	0.47	0.3	[39]
BCFT10	BZCYYb1711	16	H_2/3%H_2O–air	1.05	0.74	0.48	[42]
BCFZY	BZCYYb1711	17	H_2/air	0.66	0.53	0.42	[19]
SCFN	BZCYYb1711	26	H_2/Air	0.53	0.35	0.23	[45]
PCO-LSCF	BZCYYb4411	12	3%H_2O-H_2/3%H_2O–air	0.8	0.53	/	[47]

Electrolytes: BZCYYb1711: $BaZr_{0.1}Ce_{0.7}Y_{0.1}Yb_{0.1}O_{3-\delta}$; BZCYYb4411: $BaZr_{0.4}Ce_{0.4}Y_{0.1}Yb_{0.1}O_{3-\delta}$;

Oxygen electrode: PNCO-64: $Pr_2Ni_{0.6}Co_{0.4}O_{4-\delta}$; PBCFS05: $Pr_{0.5}Ba_{0.5}Co_{0.7}Fe_{0.25}Sn_{0.05}O_{3+\delta}$; PBCC-BCO: $PrBa_{0.8}Ca_{0.2}Co_2O_{5+\delta}$;

PBCsC: $PrBa_{0.9}Cs_{0.1}Co_2O_{5+\delta}$; BCFZYMg: $Ba(Co_{0.4}Fe_{0.4}Zr_{0.1}Y_{0.1})_{0.95}Mg_{0.05}O_{3-\delta}$; BSCFP0.05: $Ba_{0.5}Sr_{0.5}(Co_{0.8}Fe_{0.2})_{0.95}P_{0.05}O_{3-\delta}$;

BB-OPS: $Ba_{0.5}Sr_{0.5}Co_{0.8}Fe_{0.2}O_{3-\delta}$-$BaZr_{0.1}Ce_{0.7}Y_{0.1}Yb_{0.1}O_{3-\delta}$; N-BCFZYNF: $Ba(Co_{0.4}Fe_{0.4}Zr_{0.1}Y_{0.1})_{0.95}Ni_{0.05}F_{0.1}O_{2.9-\delta}$;

PSFN/Fe_2O_3: $Pr_{0.4}Sr_{0.6}Fe_{0.9}Nb_{0.1}O_{3-\delta}$/$Fe_2O_3$; D-SFN: $Sr_{2.8}Fe_{1.8}Nb_{0.2}O_{7-\delta}$; PBSCF: $PrBa_{0.5}Sr_{0.5}Co_{1.5}Fe_{0.5}O_{5+\delta}$;

BSCFF: $Ba_{0.5}Sr_{0.5}Co_{0.8}Fe_{0.2}O_{2.9-\delta}F_{0.1}$; BCFT10: $Ba(Co_{0.7}Fe_{0.3})_{0.9}Ta_{0.1}O_{3-\delta}$; BCFZY: $BaCo_{0.4}Fe_{0.4}Zr_{0.1}Y_{0.1}O_{3-\delta}$

SCFN: $Sr_{0.9}Ce_{0.1}Fe_{0.8}Ni_{0.2}O_{3-\delta}$; PCO-LSCF: $PrCoO_{3-\delta}$-$La_{0.6}Sr_{0.4}Co_{0.2}Fe_{0.8}O_{3-\delta}$

Table S9. Current density of different oxygen electrodes operating in the PCEC mode at 500–600 °C with an applied voltage of 1.3 V.

Oxygen electrode	Electrolyte	thickness (μm)	Atmosphere	Current density@1.3 V (A cm^{-2})			Refs.
				600 °C	550 °C	500 °C	
PNCO-64	BZCYYb1711	10	3%H_2O–air	1.81	0.85	/	[8]
PBCFS05	BZCYYb4411	6-7	3%H_2O–air	1.79	0.75	0.33	[49]
SCFN-RP	BZCYYb1711	10	20%H_2O–air	1.52	1.04	0.64	This work
PBCC-BCO	BZCYYb1711	10	3%H_2O–air	1.51	0.69	/	[33]
PBCsC	BZCYYb1711	8	3%H_2O–air	1.48	0.71	0.31	[48]
BCFZYMg	BZCYYb1711	16	10%H_2O–air	1.24	0.84	0.54	[43]
BB-OPS	BZCYYb1711	22	10%H_2O–air	1.1	0.67	0.47	[44]
N-BCFZYNF	BZCYYb1711	10.79	3%H_2O–air	1.09	0.68	0.35	[40]
BSCFP0.05	BZCYYb1711	16	10%H_2O–air	1	0.62	0.4	[23]
PSFN/Fe_2O_3	BZCYYb1711	10	10%H_2O–air	0.91	0.55	/	[46]
D-SFN	BZCYYb1711	23	3%H_2O–air	0.81	0.57	0.29	[28]
PBSCF	BZCYYb4411	15	3%H_2O–air	1.42	0.75	0.38	[41]
BSCFF	BZCYYb1711	16.6	3%H_2O–air	0.59	0.32	0.19	[39]
BCFT10	BZCYYb1711	16	3%H_2O–air	0.57	0.32	/	[42]
BCFZY	BZCYYb1711	11	10%H_2O–air	1.01	0.76	0.62	[19]
SCFN	BZCYYb1711	26	3%H_2O–air	0.27	0.18	0.09	[45]
PCO-LSCF	BZCYYb4411	12	30%H_2O–air	1.22	0.59	/	[47]

Electrolytes: BZCYYb1711: $BaZr_{0.1}Ce_{0.7}Y_{0.1}Yb_{0.1}O_{3-\delta}$; BZCYYb4411: $BaZr_{0.4}Ce_{0.4}Y_{0.1}Yb_{0.1}O_{3-\delta}$;

Oxygen electrode: PNCO-64: $Pr_2Ni_{0.6}Co_{0.4}O_{4-\delta}$; PBCFS05: $Pr_{0.5}Ba_{0.5}Co_{0.7}Fe_{0.25}Sn_{0.05}O_{3+\delta}$; PBCC-BCO: $PrBa_{0.8}Ca_{0.2}Co_2O_{5+\delta}$;

PBCsC: $PrBa_{0.9}Cs_{0.1}Co_2O_{5+\delta}$; BCFZYMg: $Ba(Co_{0.4}Fe_{0.4}Zr_{0.1}Y_{0.1})_{0.95}Mg_{0.05}O_{3-\delta}$; BSCFP0.05: $Ba_{0.5}Sr_{0.5}(Co_{0.8}Fe_{0.2})_{0.95}P_{0.05}O_{3-\delta}$;

BB-OPS: $Ba_{0.5}Sr_{0.5}Co_{0.8}Fe_{0.2}O_{3-\delta}$-$BaZr_{0.1}Ce_{0.7}Y_{0.1}Yb_{0.1}O_{3-\delta}$; N-BCFZYNF: $Ba(Co_{0.4}Fe_{0.4}Zr_{0.1}Y_{0.1})_{0.95}Ni_{0.05}F_{0.1}O_{2.9-\delta}$;

PSFN/Fe_2O_3: $Pr_{0.4}Sr_{0.6}Fe_{0.9}Nb_{0.1}O_{3-\delta}$/$Fe_2O_3$; D-SFN: $Sr_{2.8}Fe_{1.8}Nb_{0.2}O_{7-\delta}$; PBSCF: $PrBa_{0.5}Sr_{0.5}Co_{1.5}Fe_{0.5}O_{5+\delta}$;

BSCFF: $Ba_{0.5}Sr_{0.5}Co_{0.8}Fe_{0.2}O_{2.9-\delta}F_{0.1}$; BCFT10: $Ba(Co_{0.7}Fe_{0.3})_{0.9}Ta_{0.1}O_{3-\delta}$; BCFZY: $BaCo_{0.4}Fe_{0.4}Zr_{0.1}Y_{0.1}O_{3-\delta}$

SCFN: $Sr_{0.9}Ce_{0.1}Fe_{0.8}Ni_{0.2}O_{3-\delta}$; PCO-LSCF: $PrCoO_{3-\delta}$-$La_{0.6}Sr_{0.4}Co_{0.2}Fe_{0.8}O_3$